Supporting information for

Optimized cation exchange for mercury chalcogenides 2D nanoplatelets and its application for alloys

Corentin Dabard[1], Josep Planelles[2], Hong Po[1], Eva Izquierdo[3], Lina Makke[1], Charlie Gréboval[3], Nicolas Moghaddam[1], Adrien Khalili[3], Tung Huu Dang[3], Audrey Chu[3], Stefano Pierini[3], Claire Abadie[3], Mariarosa Cavallo[3], Erwan Bossavit[3], Xiang Zhen Xu[1], Philippe Hollander[4], Mathieu Silly[4], Emmanuel Lhuillier[3], Juan I. Climente[2,] Sandrine Ithurria[1]*

[1] Laboratoire de Physique et d'Etude des Matériaux, ESPCI-Paris, PSL Research University, Sorbonne Université Univ Paris 06, CNRS UMR 8213, 10 rue Vauquelin 75005 Paris, France.
[2]Departament de Quimica Fisica i Analitica, Universitat Jaume I, E-12080, Castello de la Plana, Spain
[3] Sorbonne Université, CNRS, Institut des NanoSciences de Paris, INSP, 75005 Paris, France.
[4]Synchrotron-SOLEIL, Saint-Aubin, BP48, F91192 Gif sur Yvette Cedex, France.

*To whom correspondence should be sent: sandrine.ithurria@espci.fr

Table of content

1. CdSeTe NPLs growth 2
2. Optimized cation exchange procedure 4
3. Alloyed $HgSe_{1-x}Te_x$ NPLs 8
4. kp Modelling of HgTe and HgSe NPL 12
5. Band alignment of $HgSe_{1-x}Te_x$ NPL 15
6. REFERENCES 17

1. CdSeTe NPLs growth

Figure S 1 and **Table S 1** summarized the spectroscopic properties of the $CdSe_{1-x}Te_x$ NPLs used as building blocks to obtain, after cation exchange, $HgSe_{1-x}Te_x$ NPLs.

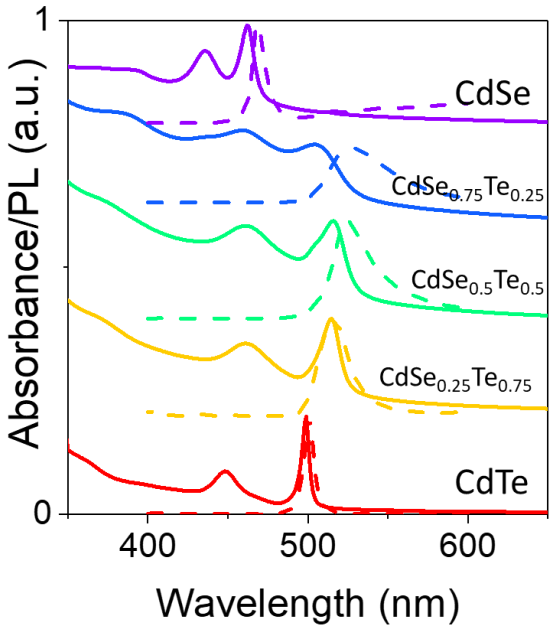

Figure S 1 Spectroscopic properties of $CdSe_{1-x}Te_x$ NPLs. *Absorption (solid lines) and PL (dashed lines) spectra of $CdSe_{1-x}Te_x$ NPLs with various compositions. For sake of clarity the spectra of various compositions have been vertically shifted.*

Table S 1 Spectroscopic properties of $CdSe_{1-x}Te_x$ NPLs. *QY stands for quantum yield, while FWHM means full width at half maximum.*

Cd	**CdTe**		**$CdSe_{0.25}Te_{0.75}$**		**$CdSe_{0.5}Te_{0.5}$**		**$CdSe_{0.75}Te_{0.25}$**		**CdSe**	
	nm	eV	nm	eV	nm	eV	nm	eV	nm	eV
Abs. Max.	500	2.47	513	2.41	516	2.39	505	2.45	462	2.67
Em. Max.	501	2.46	516	2.39	525	2.35	526	2.35	469	2.63
QY	1%		<1%		2%		5%		3%	
Stokes shift	4.9 meV		14 meV		41 meV		97.6 meV		39.9 meV	

FWHM	30 meV	100 meV	130 meV	190 meV	50 meV

2. Optimized cation exchange procedure

Figure S 2 shows TEM images of $HgSe_{0.5}Te_{0.5}$ NPLs while the cation exchange procedure is conducted in various solvents.

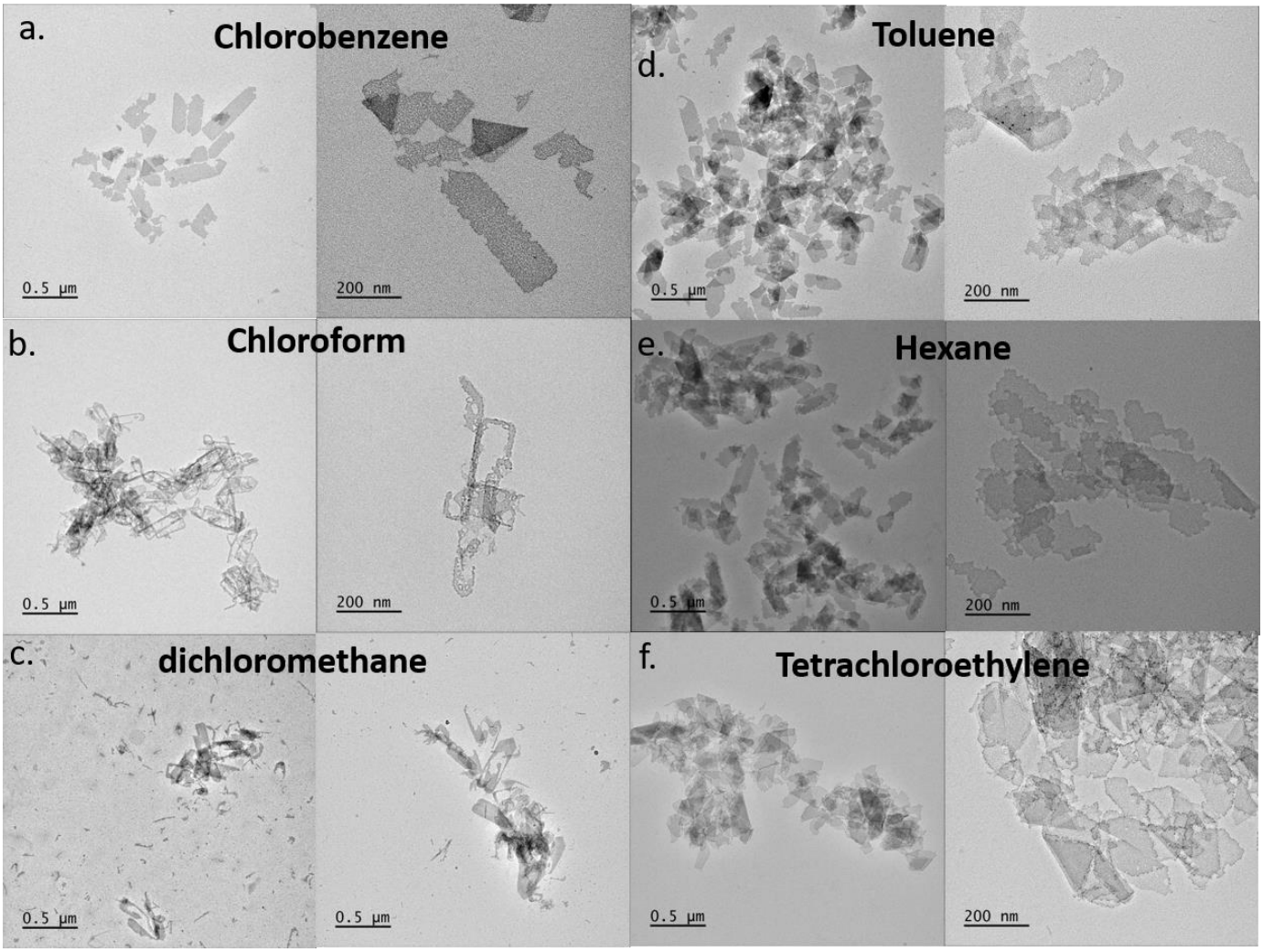

***Figure S 2 Effect of solvent on cation exchange procedure**. TEM images of $HgSe_{0.5}Te_{0.5}$ NPLs while the cation exchanged procedure is conducted in various solvents.*

Figure S 3 shows the kinetic of the cation exchange procedure while the latter is conducted in various solvents. Compared to hexane and toluene the recovering duration of the exciton for HgSe is much slower with TCE. In addition with toluene, we observe a small shoulder at 850 nm, just above the exciton of HgSe, which can be seen as the signature of a side population.

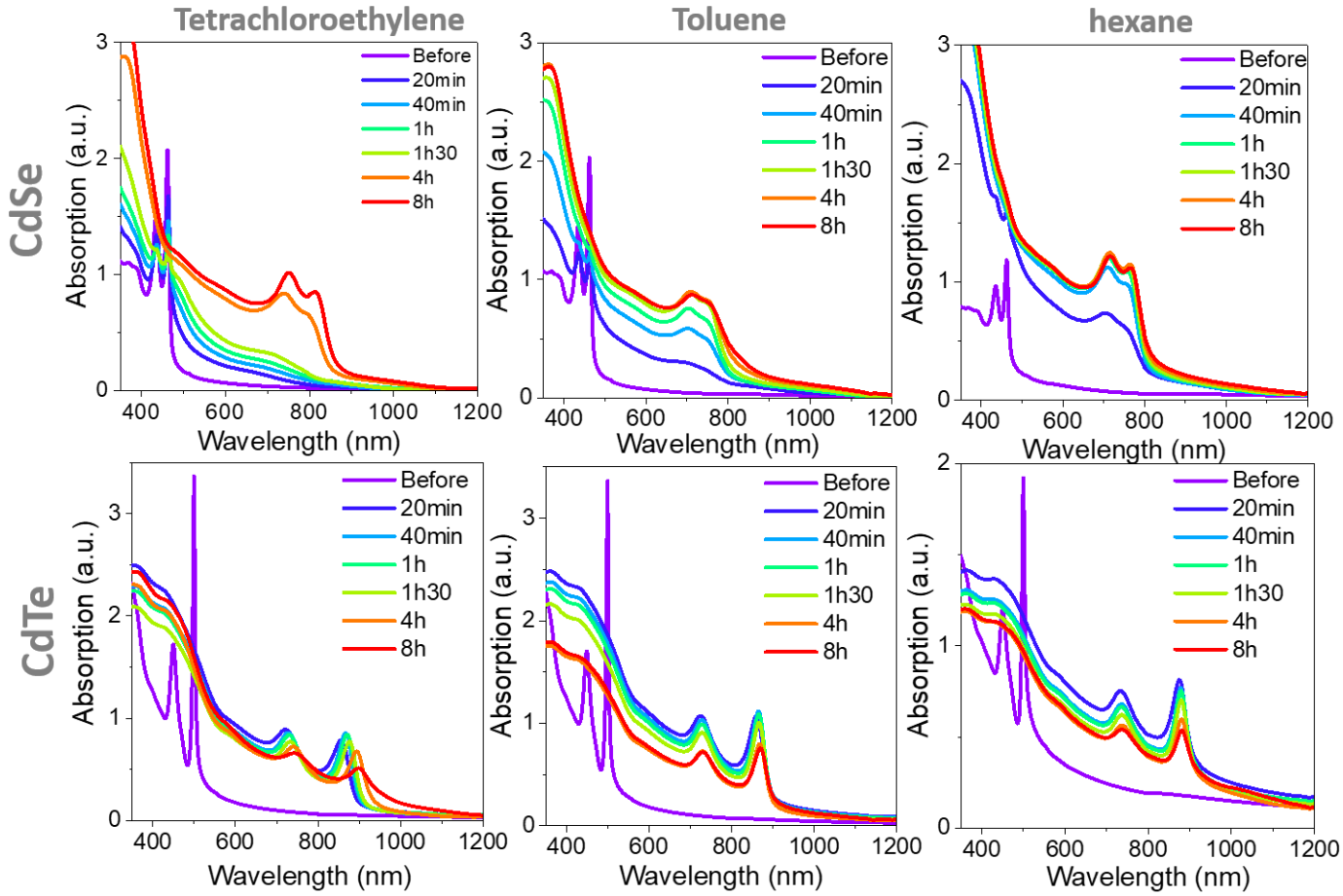

Figure S 3 Kinetic of the cation exchange for various solvents*. Absorption spectra at different time of the cation exchange reaction for CdSe NPLs (top line) and CdTe NPLs (bottom line) while the reaction is conducted in various solvents tetrachloroethylene (left column), toluene (middle column) and hexane (right column)*

Figure S 4 highlights the kinetic freeze observed when the temperature decreases by comparing the evolution of the reaction at low temperature and at room temperature. Cation exchange is carried out in two steps, first the sample is kept at -20°C for 14 days (blue and green curves) before an increase of the temperature up to room temperature for 1h (red curve). While the blue and green curves still exhibit featured of the initial NPLs of CdTe (at 500nm), the red curve does not present this signature and clear peaks coming from the Hg-based NPLs are observed (around 900 nm).

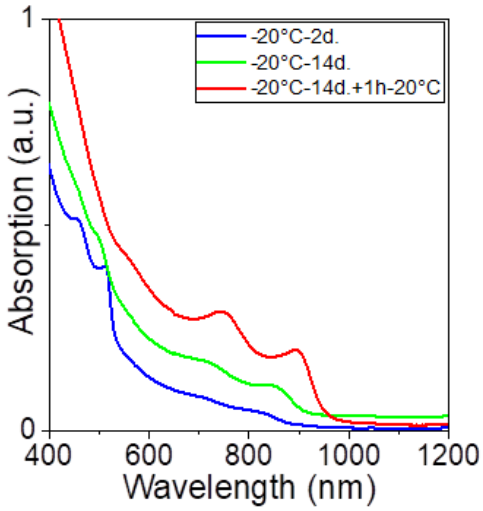

***Figure S 4 Kinetic freeze of the cation exchange procedure**. Absorption spectra after 2 days (resp. 14 days) at -20°C (blue curve (resp. green curve) and after an additional 1h at room temperature (red curve).*

Figure S 5a shows the effect of temperature and presence of oleic acid or oleate on the $HgSe_{0.5}Te_{0.5}$ NPLs absorption spectra before and after they get washed. **Figure S 5**b-c compares the TEM images of the $HgSe_{0.5}Te_{0.5}$ NPLs while the cation exchange is conducted without or with oleic acid.

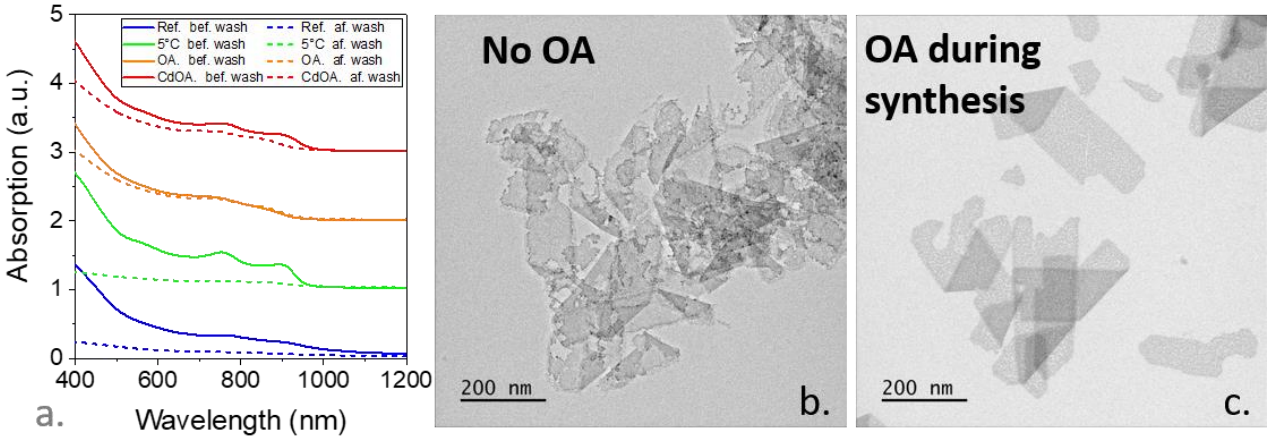

***Figure S 5 Benefit of oleic acid during cation exchange procedure**. a. Absorption spectra before and after washing of $HgSe_{0.5}Te_{0.5}$ NPLs using procedure from ref 1, while reducing the temperature (5°C instead of room temperature for reference procedure), while adding oleic acid and while adding cadmium oleate (at room temperature). b. TEM image of $HgSe_{0.5}Te_{0.5}$ NPLs while cation exchange is conducted using procedure from ref 1. c. TEM image of $HgSe_{0.5}Te_{0.5}$*

NPLs while cation exchange is conducted, at room temperature, while adding oleic acid during the procedure.

Figure S 6 shows how the dynamics of the cation exchange procedure is affected by the presence of oleate during the reaction.

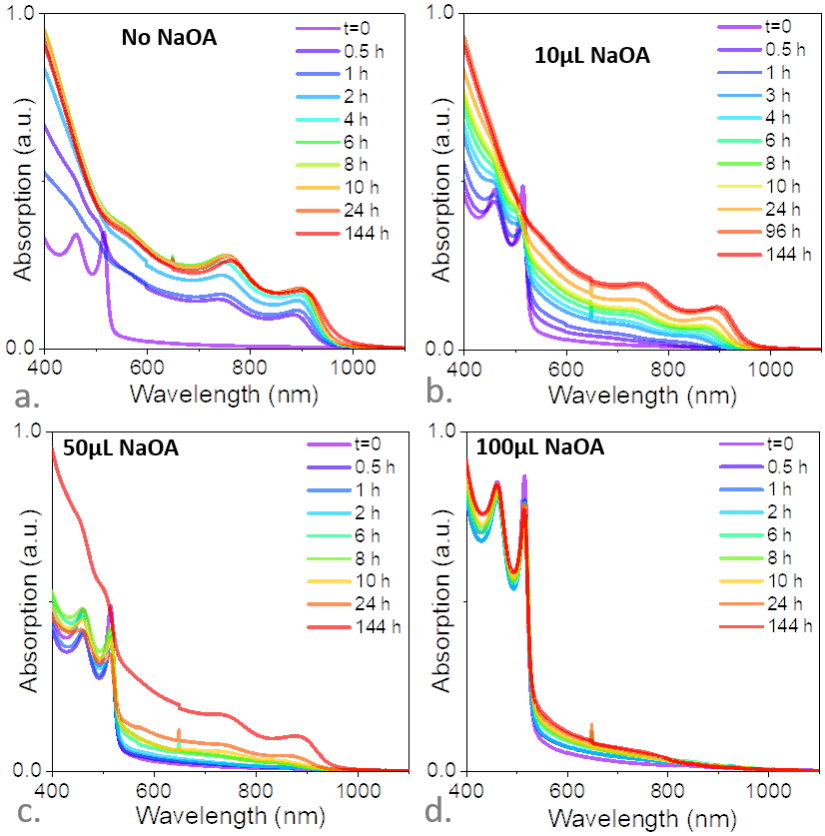

***Figure S 6 Optimization of the oleate content during cation exchange procedure**. Spectra after various durations of the cation exchange procedure for $HgSe_{0.5}Te_{0.5}$ NPLs and while no sodium oleate (a.), 10 µL of sodium oleate (0.1M in oleic acid) (b.), 50 µL of sodium oleate (0.1M in oleic acid)(c) and 100 µL of sodium oleate (0.1M in oleic acid) (d.) are added.*

3. Alloyed $HgSe_{1-x}Te_x$ NPLs

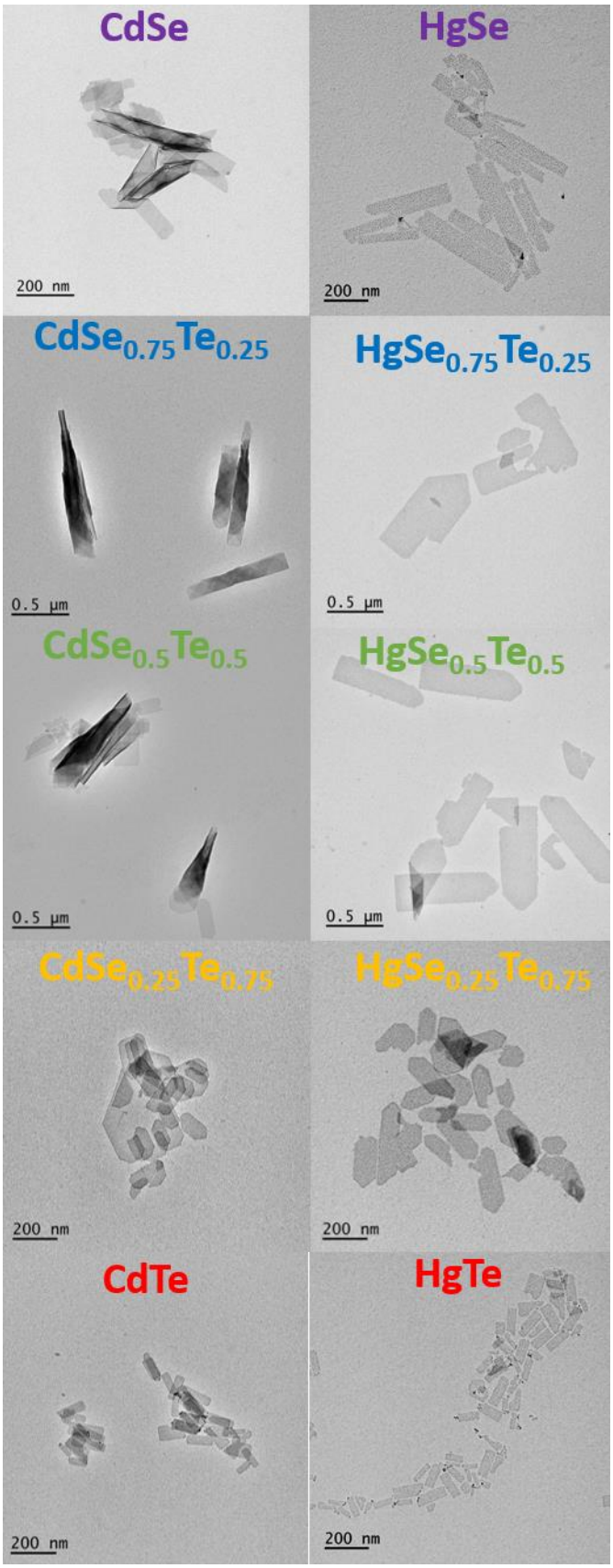

Figure S 7 TEM images of the $CdSe_{1-x}Te_x$ (left) and $HgSe_{1-x}Te_x$ (right) NPLs before and after cation exchange *for various Te contents.*

The **Figure S 7** shows the TEM image of the $CdSe_{1-x}Te_x$ and $HgSe_{1-x}Te_x$ NPLs for various compositions. It is worth noting that Hg based NPLs have reduced enrollment compared to their Cd based counterpart.

The ***Figure S 8*** highlights the influence of the alloy composition on the cation exchange speed. As the ratio of Te increase, the lattice parameter becomes larger and make easier the diffusion of the cations through the anion lattice. When comparing Figure S6a and S6b, we clearly observe this trend as the excitonic features of the initial NPLs (resp. final NPLs) decrease (resp. increase) faster in the case of the richer in Te alloys.

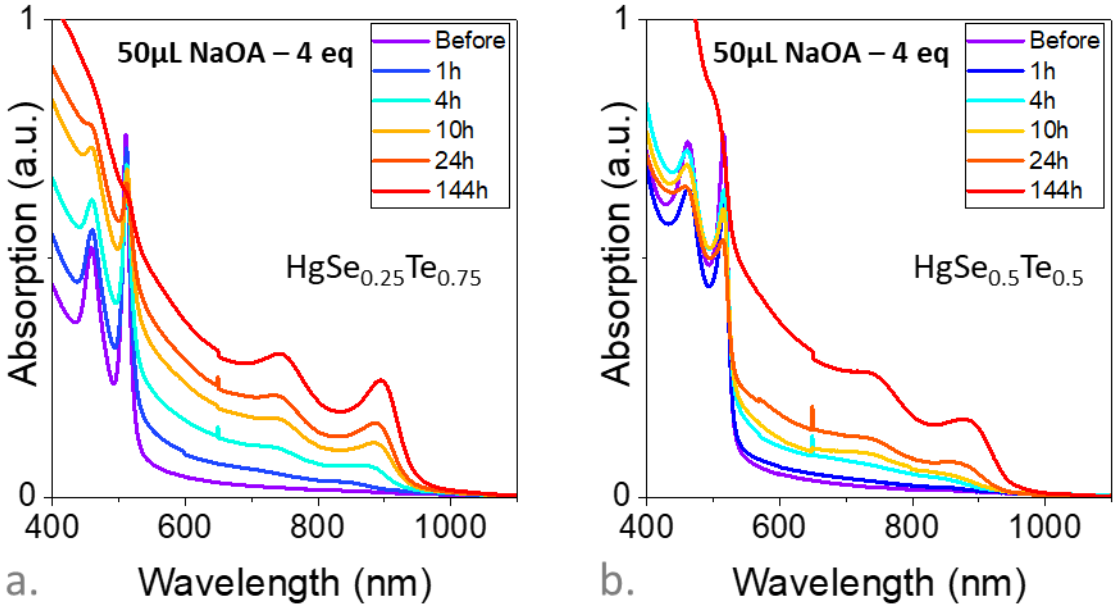

Figure S 8 Evolution of the cation exchange speed with the Te content: *a. Absorption spectra taken at different time during the cation exchange of $CdSe_{0.25}Te_{0.75}$ NPLs. b. Absorption spectra taken at different time during the cation exchange of $CdSe_{0.5}Te_{0.5}$ NPLs.*

Table S 2 Spectroscopic properties of $HgSe_{1-x}Te_x$ NPLs. *QY stands for quantum yield, while FWHM means full width at half maximum.*

Hg	HgTe		$HgSe_{0.25}Te_{0.75}$		$HgSe_{0.5}Te_{0.5}$		$HgSe_{0.75}Te_{0.25}$		HgSe	
	nm	eV	nm	eV	nm	eV	nm	eV	nm	eV
Abs. Max.	880	1.40	900	1.38	894	1.39	870	1.43	806	1.53
Em. Max.	912	1.35	933	1.32	928	1.33	922	1.34	818	1.51
QY	15%		12%		10%		2%		5%	
Stokes shift	49 meV		50 meV		50 meV		80 meV		23 meV	
FWHM	80 meV		90 meV		90 meV		210 meV		150 meV	

Estimation of the bowing parameter

The band gap values as a function of the Se content deviate from a linear law as shown in **Figure S 9**. Using the following equation $E_{SeTe} = E_{Se}x + E_{Te}(1-x) - bx(1-x)$, one can extract the bowing parameter b=0.36 eV.

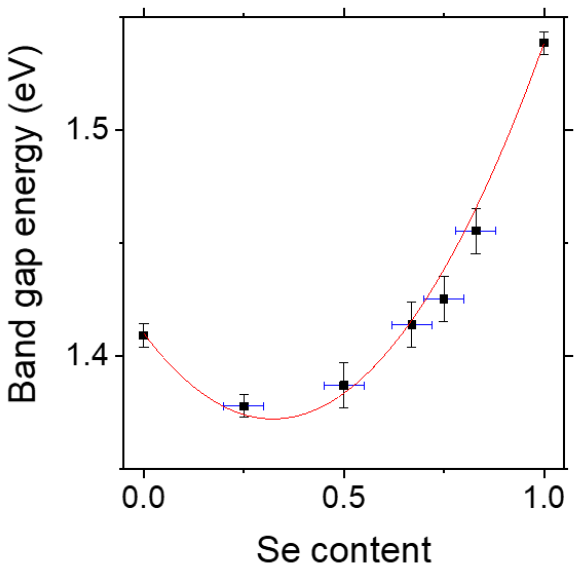

Figure S 9 Band gap of the $HgSe_{1-x}Te_x$ NPL as a function of the Se content. The scatters are the experimental data. The red line is the fit obtained from the equation $E_{SeTe} = E_{Se}x + E_{Te}(1-x) - bx(1-x)$

Figure S 10 summarizes the core level analysis of the Hg 4f, Te 4d and Se 3d states for all the investigated composition of $HgSe_{1-x}Te_x$ NPLs.

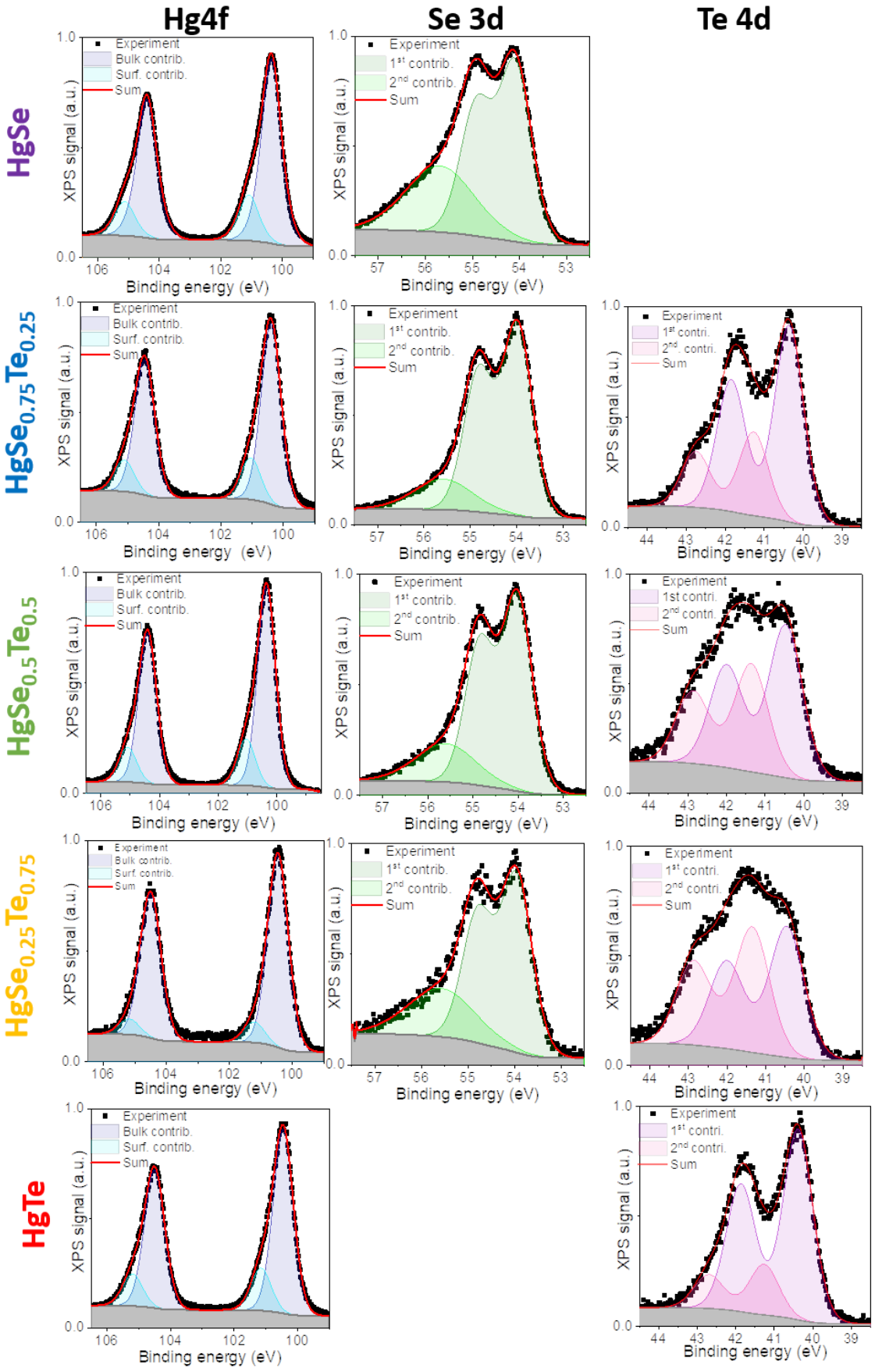

Figure S 10 Core level analysis for $HgSe_{1-x}Te_x$ NPLs revealed by X -ray photoemission. *Hg 4f, Se 3d and Te 4d core level for $HgSe_{1-x}Te_x$ NPLs with various compositions.*

4. kp Modelling of HgTe and HgSe NPL

Within an 8-band k·p Hamiltonian, the wave function is a spinorial object the form $\Psi(r) = \sum_{n=1}^{8} f_n(r)\, u_n(r)$, where $f_n(r)$ is the envelope function associated to the periodic Bloch function $u_n(r)$. For the subband edge (k_x=k_y=*0*), however, the HH band remains decoupled, while E, LH and SO bands with the same spin couple among themselves[2]. We thus have multi-component states such as:

$$\Psi(r) = f_1(r)\, u_1(r) + f_5(r)\, u_5(r) + f_7(r)\, u_7(r),$$

$$\Psi(r) = f_2(r)\, u_2(r) + f_6(r)\, u_6(r) + f_8(r)\, u_8(r),$$

for E-LH-SO subbands, or states such as:

$$\Psi(r) = f_3(r)\, u_3(r),$$

$$\Psi(r) = f_4(r)\, u_4(r),$$

for the HH subbands. As mentioned in Methods, $u_1(r) = |\Gamma_6, +1/2\rangle$ and $u_2(r) = |\Gamma_6, -1/2\rangle$ are the "electron" bands, $u_3(r) = |\Gamma_8, +3/2\rangle$ and $u_4(r) = |\Gamma_8, -3/2\rangle$ the heavy hole bands, $u_5(r) = |\Gamma_8, +1/2\rangle$ and $u_6(r) = |\Gamma_8, -1/2\rangle$ the light hole bands, and $u_7(r) = |\Gamma_7, +1/2\rangle$ and $u_8(r) = |\Gamma_7, -1/2\rangle$ the split-off bands. $f_n(r)$ are the associated envelope functions, and the normalized weight of the *n*-th band within the spinor can be estimated from $\langle f_n | f_n \rangle$.

Figure S 11 shows the energy and band composition of HgTe (**Figure S 11**a-c) and HgSe (**Figure S 11**d-f) quantum wells, calculated with an 8-band k·p model, including quantum confinement along the *z* ([001]) direction, and keeping k_x=k_y=0 in-plane. Both materials exhibit similar dependence on the well thickness, with a transition from semimetal to semiconductor at thickness L_z≈6 nm, and band gaps of 1.3-1.4 eV at L_z =1 nm, see **Figure S 11**a and d.

The first subband of the conduction band, which we label as ①, has an increasing Γ_6 character (labeled as E in **Figure S 11**b and e) with increasing confinement. For the NPLs we synthesized, which have L_z≈1 nm, the normalized weight is ≈0.85. This is very different from the case of thicker quantum wells, with L_z=6-8 nm (this is the usual regime of epitaxial quantum wells), where E and LH bands have comparable contributions (≈0.50 each for L_z=8 nm).

In the valence band, the first subband (black line in **Figure S 11** a,d) is a pure HH. The next subband, labeled as ②, has a clearly dominant LH character for thin NPL throughout the region under study (see green line in **Figure S 11**c,f), but again the mixing with E increases for thicker structures.

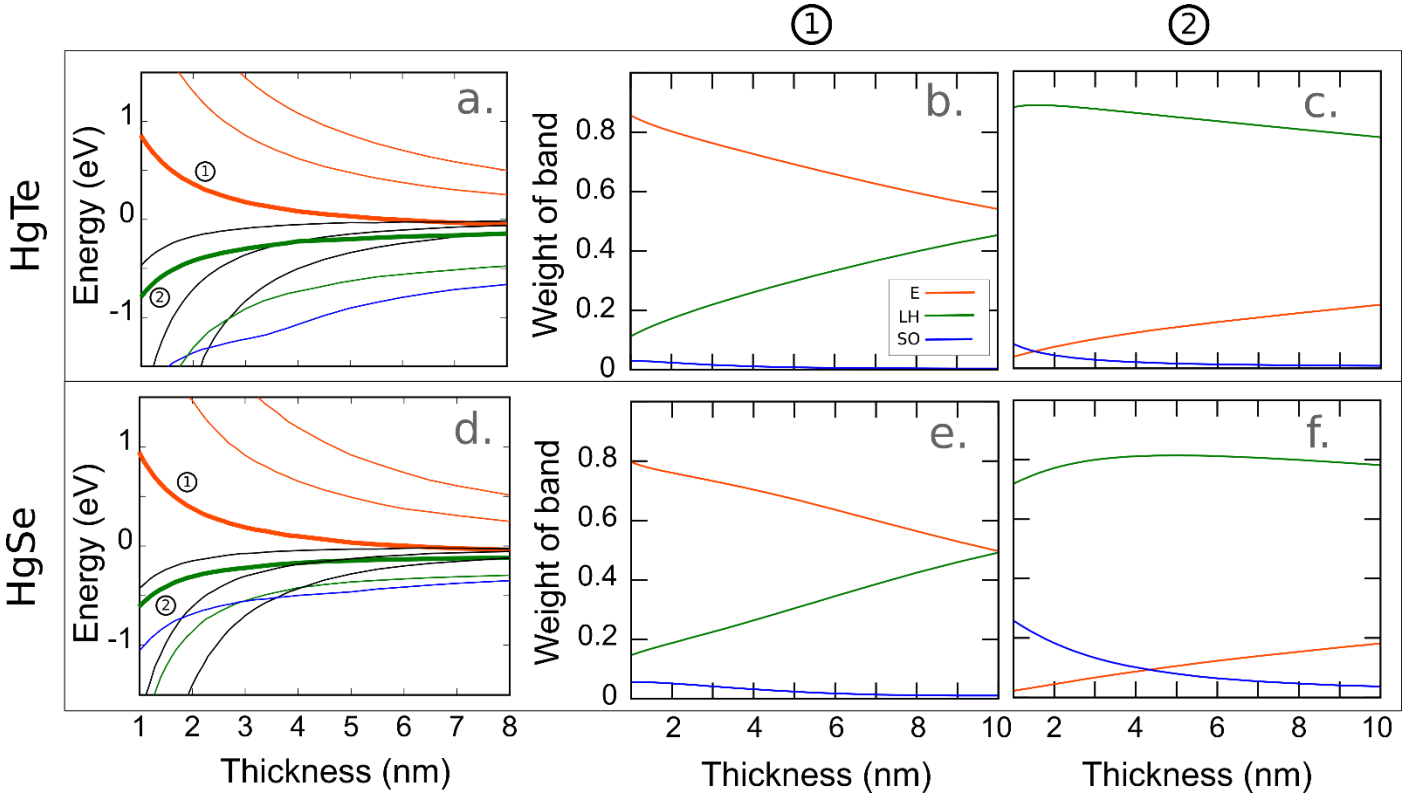

Figure S 11 Calculated subbands of HgSe and HgTe quantum wells*. Energy of HgTe subbands (a) and band composition of the subbands labeled as ① (b) and ② (c), as a function of the quantum well thickness. (d-f): same but for HgSe.*

Insight into the multiband wave functions of HgTe quantum wells is given in **Figure S 12**. In the figure, the wave function of the first states above and below the Fermi level are shown for thin (L_z*=1* nm, left column) and thick (L_z*=8* nm, right column) quantum wells. Again, the subband edge (k_x=k_y*=0*) is considered in all instances.

As mentioned in **Figure 4**b of the main text and in **Figure S9**, for a thin NPL the first conduction band state has a dominant E band character. This can be seen in the top-left panel of Figure S9bis. The main component of the multi-band wave function is the E band, nodeless (n=0, *s*-like) envelope function (orange line in the top-left panel). In addition, small contributions of LH and SO bands, with *p*-like (*n=1*) envelope function (green and blue lines, respectively) are also observed. Yet, because the weight of the E band component is clearly dominant, in the main text we simplify the notation by labeling this state as the *E(n=0)* subband.

For the same thickness, L_z*=1* nm, the top of the valence band is formed by a pure *HH(n=0)* subband (mid-left panel in **Figure S 12**) - because there is no coupling of HH to near bands for k_x=k_y*=0*. This subband is followed by a state (bottom-left panel) with dominant *s*-like LH character (green line), and small contributions of E and SO bands, which we label as *LH(n=0)* subband.

The effect of the NPL thickness on the band mixing can be visualized by comparing left (L_z*=1* nm) and right (L_z=8 nm) panels in **Figure S 12**. In a thick NPL, the E(*n=0*) state (top-right panel) and LH(n=0) states already displays comparable E and LH amplitudes.

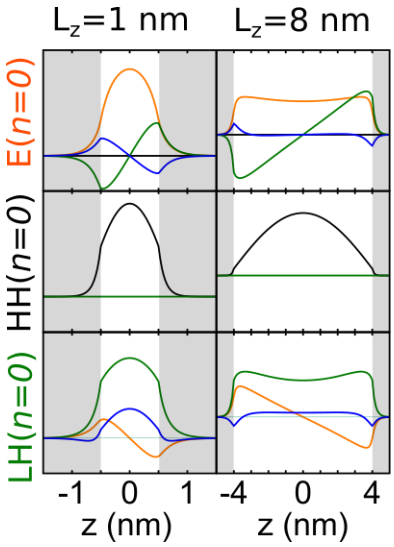

Figure S 12 Wave function of the first subband edges in HgTe quantum wells. *For every state $\Psi(r)$, the different contributing envelope functions $f_n(r)$, are represented. Orange: $f_1(r)$ (E band). Black: $f_3(r)$ (HH band). Green: $f_5(r)$ (LH band). Blue: $f_7(r)$ (SO band).*

5. Band alignment of $HgSe_{1-x}Te_x$ NPL

Figure S 13 shows the effect of thiol ligand exchange on the absorption spectra of $HgSe_{1-x}Te_x$ NPLs, presenting a clear redshift with respect to the same material capped by oleate and oleylamine. **Figure S 14** provides the secondary electron cut-off spectra and valence band spectra from X -ray photoemission of $HgSe_{1-x}Te_x$ NPLs with various compositions. Finally, **Table S 3** summarizes band alignment parameters for $HgSe_{1-x}Te_x$ NPLs

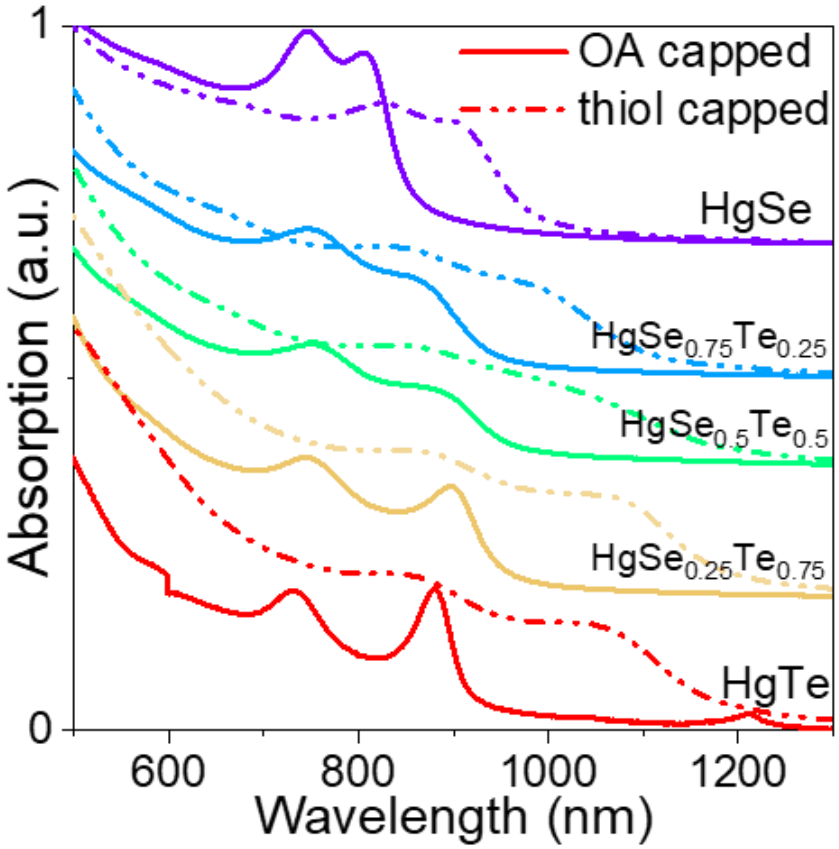

Figure S 13 Absorption spectra of $HgSe_{1-x}Te_x$ NPL with thiol capping. *Absorption spectra of $HgSe_{1-x}Te_x$ NPLs with various compositiosn while the NPLs are capped with oleates (full lines) and with thiols (dashed lines).*

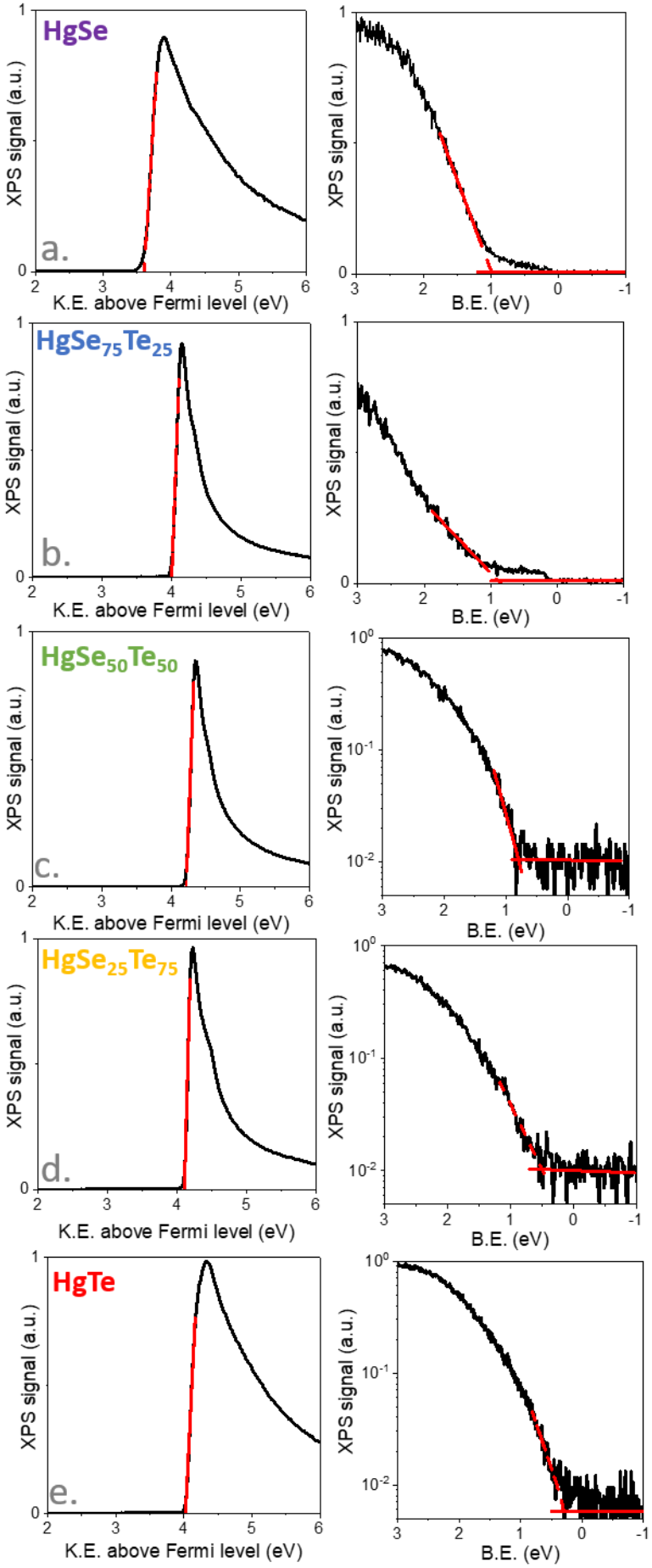

Figure S 14 Band alignment revealed by photoemission for $HgSe_{1-x}Te_x$ NPLs. *X-ray photoemission signal relative to (left) secondary electron cut-off and (right) and valence band for*

HgSe NPLs (a.), $HgSe_{0.75}Te_{0.25}$ NPLs (b.), $HgSe_{0.5}Te_{0.5}$ NPLs (c.), $HgSe_{0.25}Te_{0.75}$ NPLs (d.), HgTe NPLs (e.). KE stands for kinetic energy while BE stands for binding energy.

Table S 3 Band alignment parameters *(energy of the valence band with respect to Fermi level, work function and band gap)* ***of $HgSe_{1-x}Te_x$ NPLs*** *with various compositions with thiol capping. All numbers are given in eV.*

	HgTe	**$HgSe_{0.25}Te_{0.75}$**	**$HgSe_{0.5}Te_{0.5}$**	**$HgSe_{0.75}Te_{0.25}$**	**HgSe**
VB	0.35	0.51	0.79	0.9	1
W_F	4.02	4.10	4.22	3.99	3.6
E_g (thiol capped)	1.17	1.15	1.16	1.25	1.36

6. REFERENCES

(1) Izquierdo, E.; Robin, A.; Keuleyan, S.; Lequeux, N.; Lhuillier, E.; Ithurria, S. Strongly Confined HgTe 2D Nanoplatelets as Narrow Near-Infrared Emitters. *J. Am. Chem. Soc.* **2016**, *138*, 10496–10501.

(2) Moghaddam, N.; Gréboval, C.; Qu, J.; Chu, A.; Rastogi, P.; Livache, C.; Khalili, A.; Xu, X. Z.; Baptiste, B.; Klotz, S.; Fishman, G.; Capitani, F.; Ithurria, S.; Sauvage, S.; Lhuillier, E. The Strong Confinement Regime in HgTe Two-Dimensional Nanoplatelets. *J. Phys. Chem. C* **2020**, *124*, 23460–23468.